

Geophysical Research Letters®

RESEARCH LETTER

10.1029/2021GL095023

Key Points:

- A common index of Atlantic Multidecadal Variability (AMV) is low-pass filtered North Atlantic minus global-mean sea surface temperature (SST)
- This index aliases the structure of forced climate change onto the pattern of internal AMV in the future
- An alternative index based on removing the forced pattern of SST associated with the global-mean is generally robust to climate change

Supporting Information:

Supporting Information may be found in the online version of this article.

Correspondence to:

C. Deser,
cdeser@ucar.edu

Citation:

Deser, C., & Phillips, A. S. (2021). Defining the internal component of Atlantic Multidecadal Variability in a changing climate. *Geophysical Research Letters*, *48*, e2021GL095023. <https://doi.org/10.1029/2021GL095023>

Received 6 JUL 2021
Accepted 23 OCT 2021

Author Contributions:

Conceptualization: Clara Deser
Data curation: Adam S. Phillips
Formal analysis: Clara Deser, Adam S. Phillips
Investigation: Clara Deser
Methodology: Clara Deser
Software: Adam S. Phillips
Supervision: Clara Deser
Validation: Adam S. Phillips
Visualization: Adam S. Phillips
Writing – original draft: Clara Deser
Writing – review & editing: Clara Deser

Defining the Internal Component of Atlantic Multidecadal Variability in a Changing Climate

Clara Deser¹  and Adam S. Phillips¹ 

¹National Center for Atmospheric Research, Boulder, CO, USA

Abstract The canonical index of “Atlantic Multidecadal Variability” (AMV) is the low-pass filtered timeseries of sea surface temperature anomalies (SSTA) averaged over the North Atlantic. This index and its associated SSTA spatial pattern confound externally forced climate change and internally generated climate variability. The internal component of AMV is commonly isolated by either subtracting the global-mean SSTA or removing the pattern of SSTA associated with the global-mean. This study evaluates the skill of each method with regard to the spatial pattern of internal AMV, using nine coupled model Large Ensembles over the period 1940–2100 as a testbed in which the true internal AMV is known *a priori*. The first method aliases the structure of forced climate change onto internal AMV, while the second method is generally robust to climate change. The models simulate realistic patterns of internal AMV, although such an assessment is hampered by the brevity of the observational record.

Plain Language Summary As anthropogenic climate change escalates, conventional methods aimed at isolating modes of natural climate variability from forced changes may be inadequate. This study considers the “Atlantic Multidecadal Oscillation” (also known as “Atlantic Multidecadal Variability”), a well-known phenomenon canonically defined from the timeseries of sea surface temperatures averaged over the North Atlantic basin. A simple and widely used approach for removing the anthropogenic signal from this index and its associated spatial pattern is to subtract the global-mean temperature at each location and time. However, this method aliases the pattern of forced climate change onto the pattern of natural AMV. A simple alternative approach based on subtracting the pattern of anthropogenic climate change associated with global-mean temperature is much more successful at isolating the natural component of AMV within a background changing climate. The conclusions are based on evidence from nine different state-of-the-art coupled climate model “large ensembles,” which serve as methodological testbeds by providing robust estimates of the true structure of the models’ natural modes of variability under human-induced climate change. The results have general implications for how modes of natural variability are defined in a future warming world.

1. Introduction

The “Atlantic Multidecadal Oscillation” (also known as “Atlantic Multidecadal Variability”; AMV) is a prominent mode of low-frequency variability of the coupled ocean-atmosphere system, with climate impacts in many regions worldwide (see the recent review by Zhang et al., 2019; hereafter Z19). Originating within the Atlantic basin, this mode is thought to be initiated by low-frequency interactions between the oceanic thermohaline circulation (the Atlantic Meridional Overturning Circulation: AMOC) and the large-scale atmospheric circulation (the North Atlantic Oscillation: NAO) (e.g., Delworth et al., 2017; Kim et al., 2018; Wills et al., 2019). Coupled atmosphere-ocean mixed layer interactions also play a key role (e.g., Clement et al., 2015). At the sea surface, AMV is expressed as a basin-wide pattern of temperature anomalies generally of one sign throughout the North Atlantic (NA) and of opposite sign in the tropical South Atlantic (Z19). While many processes contribute to the formation of AMV sea surface temperature anomalies (SSTA) within the NA, ocean dynamics are a key driver in the subpolar region while atmospheric influences predominate at lower latitudes (e.g., Buckley et al., 2014; Kim et al., 2020; Wills et al., 2019).

AMV is commonly characterized with a simple SSTA index, namely the area-averaged monthly SSTA over the NA (0°–60°N and 80°W–0°; Enfield et al., 2001). To emphasize the multidecadal nature of AMV, this index is typically low-pass filtered and the secular trend removed. Some studies remove a linear trend (e.g., Bellomo et al., 2018; Enfield et al., 2001), but this procedure has been shown to alias the non-linear

component of global warming (Trenberth & Shea, 2006; hereafter, TS06; Simpson et al., 2018; Z19). An alternative approach introduced by TS06 is to subtract the global-mean SSTA (G) from the NA SSTA to derive an index of the unforced (e.g., internal) component of AMV; this method is in wide use due to its simplicity. However, by design, this approach does not account for any spatial structure in the pattern of SSTA associated with anthropogenic climate change. The degree to which such structure corrupts the spatial pattern of AMV remains an open question. Indeed, there is active debate regarding the relative contributions of external radiative forcing due to changes in anthropogenic aerosols and greenhouse gases vs. internal processes to the observed characteristics of AMV over the historical record (e.g., Bellomo et al., 2018; Booth et al., 2012; Murphy et al., 2017; Qin et al., 2020; Yan et al., 2019). It is likely that some combination of internal and external influences are present in the instrumental record of AMV (e.g., Qin et al., 2020). Paleoclimate proxy data also support the existence of internally generated AMV over at least the last millennium (Z19), although the signature of a distinct spectral peak has been questioned by Mann et al. (2020). Additionally, some state-of-the-art fully coupled climate models are able to simulate realistic AMV characteristics due to internal mechanisms alone (Z19).

In this study, we focus on the component of AMV that is internally generated (hereafter termed iAMV), and address the following questions: (1) Does the TS06 method successfully isolate iAMV in a changing climate? (2) If not, why not and when does the method start to fail? and (3) Is there a simple, alternative approach that is robust to climate change, in particular the method of removing the SSTA pattern associated with global-mean temperature (Ting et al., 2009, hereafter T09; Z19)? To answer these questions, we employ the framework of coupled model “initial-condition Large Ensembles” (LEs) for which a good estimate of the true iAMV is known *a priori*. We analyze nine different model LEs over the period 1940–2100 under historical and projected radiative forcing. Our focus is on simple SSTA-based definitions of iAMV; other, more complex statistical approaches such as those of T09, Frankignoul et al. (2017) and Wills et al. (2020) are beyond our scope.

The rest of this study is organized as follows. Section 2 describes the model and observational data sets, and methodologies. Section 3 presents an assessment of two simple methods for defining the global spatial pattern of SSTA associated with iAMV under a changing climate in nine model LEs, along with an evaluation of model fidelity that takes into account sampling uncertainty in the observational record. Section 4 provides a summary and discussion.

2. Data and Methods

2.1. Data

We make use of two gridded observational SST products updated to 2020: NOAA Extended Reconstructed Sea Surface Temperature version 5 (ERSSTv5; Huang et al., 2017) and Hadley Center Sea Ice and Sea Surface Temperature version 1 (HadISST1; Rayner et al., 2003). We analyze available Coupled Model Intercomparison Phase 5 (CMIP5) and Phase 6 (CMIP6) model LEs (see Deser et al., 2020) that contain a minimum of 30 ensemble members and simulate both the historical and future periods (the latter using either the RCP8.5, SSP5-85 or SSP3-70 radiative forcing scenario): see Table S1 in Supporting Information S1. All nine model LEs use a similar experimental design, but vary in their start dates and initial-condition perturbation methods (Table S1 in Supporting Information S1). Where possible, we discard the first 10 years of simulation to avoid potential effects of initial-condition memory, and analyze the period 1940–2100, which is generally common to all of the model LEs. All model and observational data have been bi-linearly interpolated to the Community Earth System Model version 1 (CESM1) grid for ease of comparison. All data are annual averages smoothed with a 20-year Butterworth low-pass filter (similar results are obtained using a 10-year Butterworth filter; not shown). Note that in the models, SSTA values in areas of sea ice denote the surface temperature of the ice.

2.2. Estimated iAMV

Here, we use two methods to estimate the pattern of iAMV in models and observations: (1) subtract G from the SSTA at each grid box and time step and then regress these data onto the NA-G index; and (2) subtract the *pattern* of SSTA associated with G (obtained by regressing SSTA at each location onto G, and then

scaling the pattern by the value of G at each time step) from the SSTA at each grid box and time step, and then regress these data onto the NA-G index. Method 1 is the same procedure as TS06 except for the removal of G from the gridded data; this step is necessary to avoid spurious results in models' future projections as detailed in the Supporting Information S1. Method 2 is identical to that introduced by T09 and used by Z19; note that the pattern of iAMV obtained with this method has zero global-mean component by construction. We shall refer to Method 1 as “T&S” for historical precedent, and Method 2 as “Residual” following the nomenclature of Z19.

2.3. True iAMV

With an initial-condition LE of sufficient size, it is straightforward to separate the forced component of SSTA (estimated by the ensemble-mean) from the internal component of SSTA (iSSTA; estimated as the residual from the ensemble-mean) in each member at each grid box and time step. For consistency with the methods outlined in Section 2.2, we subtract the global-mean iSSTA from iSSTA at each grid box and then regress these data onto the internal NA-G index to obtain the “true iAMV” pattern in each ensemble member. We note that this step is necessary to be able to compare directly with the patterns obtained using the methods in Section 2.2, which have zero global-mean by construction; the impact of subtracting the global-mean iSSTA on the pattern of iAMV will be reported in a separate study.

To assess the performance of the T&S and Residual methods, we compute pattern correlation coefficients and rms differences between the ensemble-means of the estimated and true iAMV regression maps using area-weighted values for all grid boxes within the domain 60°S–60°N (results for the NA region and the global domain excluding the NA are given in Supporting Information S1). Statistical significance of the iAMV regression maps is assessed using a two-sided Student t -test at the 90% confidence level, taking into account temporal autocorrelation in the low-pass filtered data.

3. Results

3.1. Spatial Patterns of Estimated and True iAMV

The estimated and true iAMV regression maps for the 100-member MPI LE during 1950–2020 and 1950–2090 are shown in Figure 1 (results for all nine model LEs including an assessment of statistical significance are shown in Figures S1–S9 in Supporting Information S1). Note that the estimated (true) iAMV regression map is the average of the 100 individual estimated (true) iAMV regression maps. In general, regression coefficients >0.4 in absolute value are statistically significant, except for portions of the Southern Ocean (Figure S1 in Supporting Information S1). The true iAMV pattern, similar for the two time periods, exhibits positive anomalies throughout the NA with the largest values in the central subpolar region and along the sea ice edge, and weaker anomalies extending into the tropics; negative anomalies are found to the south of the equator in the Atlantic sector (Figures 1c and 1d). A coherent pattern of anomalies is also evident over the Pacific sector, with positive values in the western and central North Pacific, and negative values in the eastern North Pacific extending southwestward into the tropics, with a strong resemblance to the negative phase of Pacific Decadal Variability (PDV; Newman et al., 2016). The true iAMV patterns in the other eight model LEs (Figures S2–S9 in Supporting Information S1) are similar to MPI over the Atlantic sector, and mostly similar to MPI over the Indo-Pacific sector with two exceptions (Figures S4 and S5 in Supporting Information S1).

How well can the true pattern of iAMV be estimated with the T&S and Residual methods? Results for MPI indicate that both methods perform extremely well during the period 1950–2020, with pattern correlations (r) of 1.00 and 0.99 against the truth (Figures 1a and 1e). Over the longer period 1950–2090, the Residual method remains highly skillful ($r = 0.96$; Figure 1f) while the T&S method is much less successful ($r = 0.53$) and also strongly overestimates the amplitude over the subpolar NA (Figure 1b). The degradation of the T&S method for the longer period is due to aliasing of the forced climate change pattern onto the estimated iAMV. This can be seen by the resemblance between the T&S regression map and the (oppositely signed) forced trend pattern ($r = -0.75$; Figure 1h). The climate change pattern effect is less of an issue for the historical period 1950–2020 when forced SST trends are considerably weaker and more spatially homogeneous ($r = 0.14$; Figure 1g). Unlike T&S, the Residual method explicitly accounts for the forced pattern

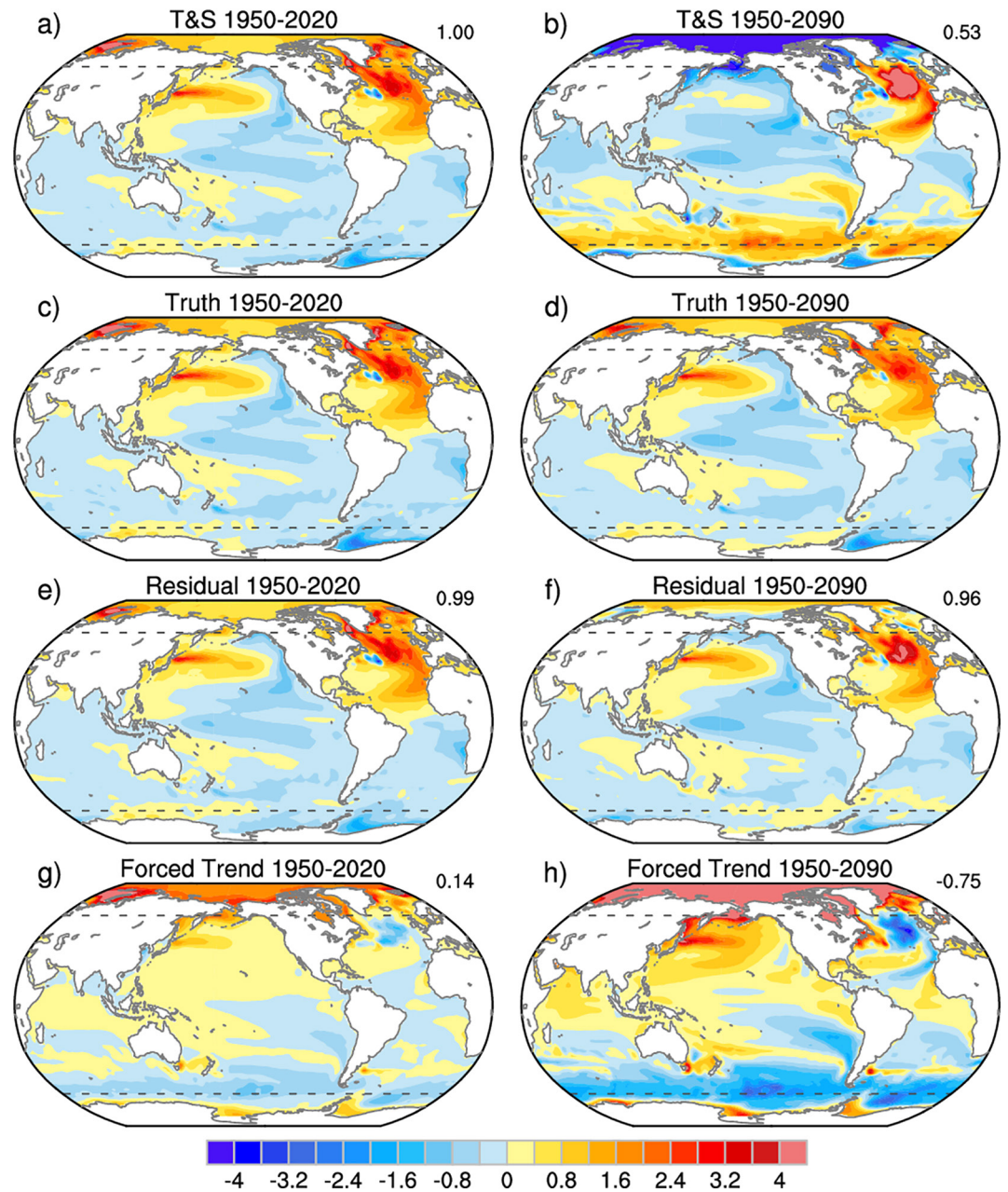


Figure 1. Sea surface temperature (SST) regression maps of internal Atlantic Multidecadal Variability (iAMV) in the 100-member MPI Large Ensemble during (left) 1950–2020 and (right) 1950–2090 estimated with the T&S (a and b) and Residual (e and f) methods; True patterns are shown in panels (c and d). Numbers in the upper right indicate the pattern correlation with the Truth for the domain 60°S–60°N (marked by dashed gray lines). The color bar is unitless (°C per °C of the iAMV index). Panels (g and h) show the forced (ensemble-mean) SST trends minus the global-mean forced trend (°C per 70 years and °C per 140 years, respectively); numbers in the upper right denote the pattern correlation with the T&S regression map.

effect; however, it too may be vulnerable if the pattern of forced climate change evolves substantially over the period of analysis (see further discussion in Section 4). The skill of the T&S and Residual methods in estimating the structure and amplitude of true iAMV (and the role of the forced SST pattern effect) in the other models is discussed in Section 3.2.

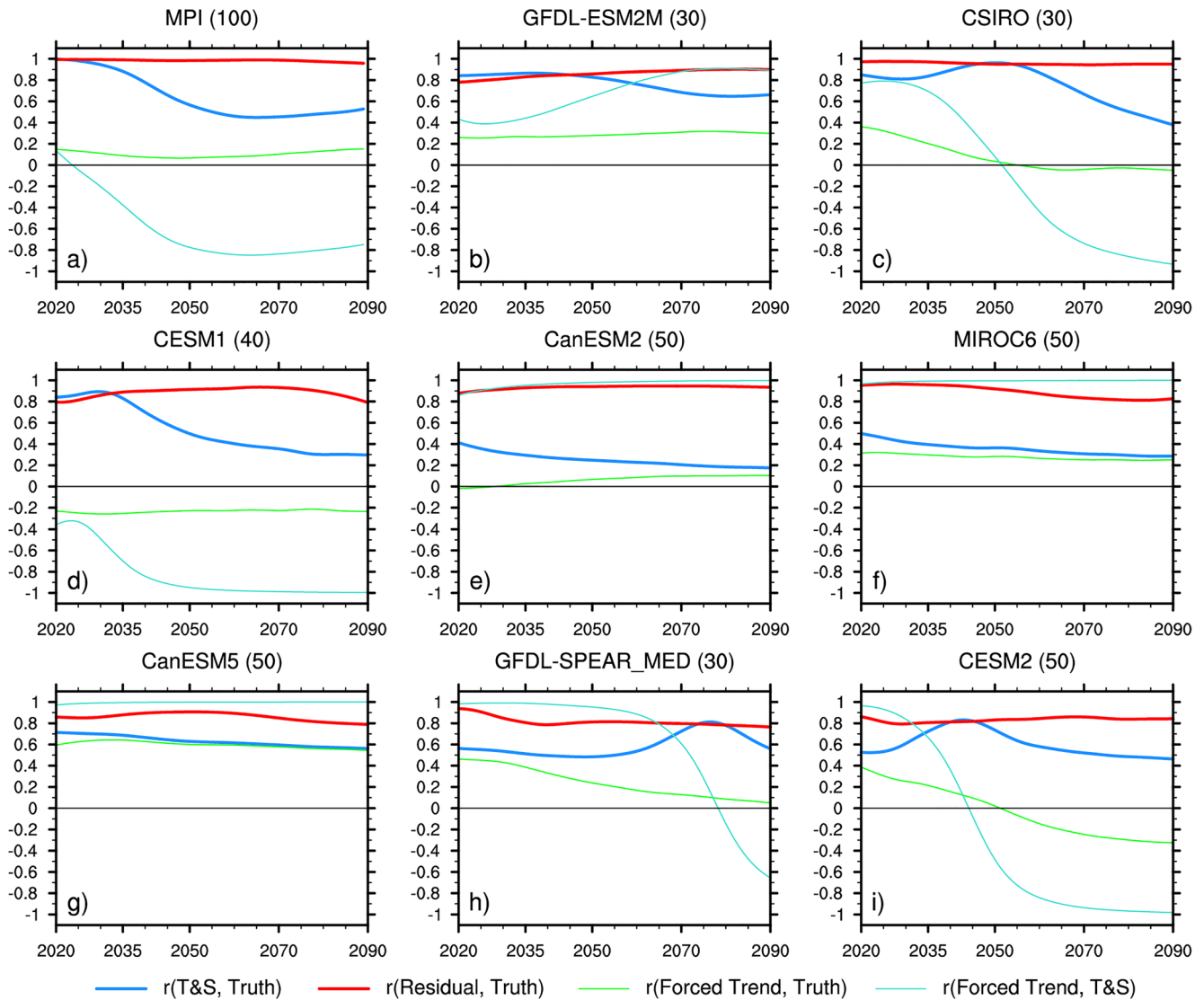


Figure 2. Cumulative pattern correlations between internal Atlantic Multidecadal Variability sea surface temperature regression maps for nine different model large ensembles: T&S versus Truth (blue curves); Residual versus Truth (red curves); Forced trend versus T&S (cyan curves); Forced trend versus Truth (green curves). The cumulative analysis periods begin in 1950 and end in the year labeled along the x-axis. Panel titles indicate the model name and number of ensemble members (see Table S1 in Supporting Information S1).

3.2. Time-Evolution of True and Estimated iAMV Patterns and Amplitudes

In the previous subsection, we established that the T&S method gives an accurate estimate of true iAMV during 1950–2020 in the MPI LE, but deteriorates considerably when the analysis period is extended to 2090. When does this degradation occur? To address this question, we repeat our analysis for all end dates between 2020 and 2090: that is, we add one year at a time to the end of our analysis period (1950–2020, 1950–2021, ..., 1950–2089, and 1950–2090) to examine the progression of the degree of resemblance between the estimated and true iAMV patterns. These “cumulative” pattern correlations between the true iAMV and the T&S estimate decline from a maximum value of 0.99 in the 2020s (years refers to the ending date of the analysis period) to a minimum value of 0.43 in the 2060s, increasing only slightly thereafter (Figure 2a, blue curve). This decline in pattern correlation is accompanied by an increase in spatial rms error (rmse) from 0.1 in the 2020s to 1.7 in the 2060s (Figure 3a, blue curve), where rmse is defined as the spatial rms of the difference between the estimated and true iAMV patterns, divided by the spatial rms of the true iAMV pattern. [For the rmse calculations, the regression maps are computed using normalized iAMV indices and then

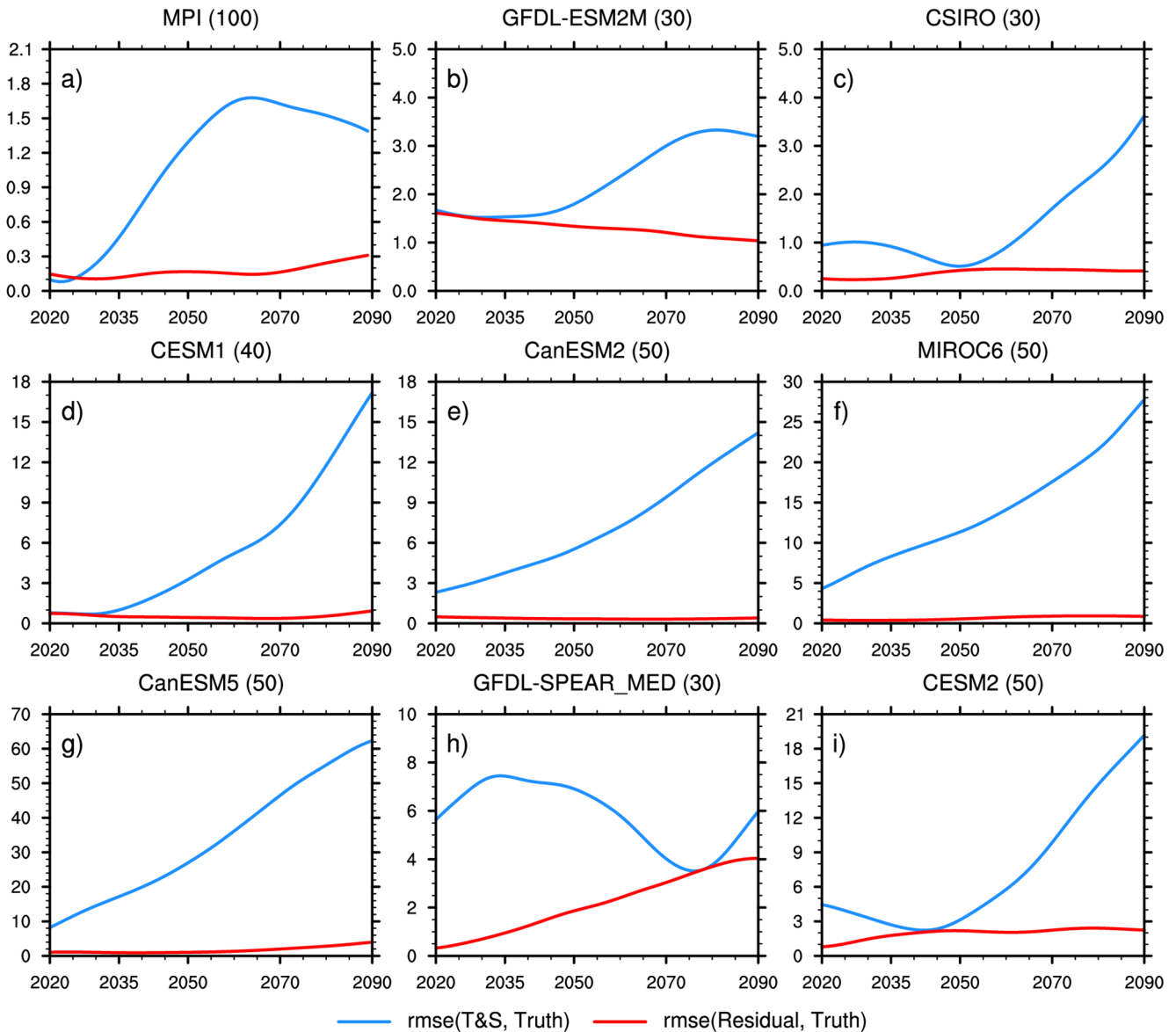


Figure 3. As in Figure 2 but for cumulative spatial rms differences relative to the spatial rms of the true internal Atlantic Multidecadal Variability (“rmse”) for each model Large Ensemble: T&S versus Truth (blue); Residual versus Truth (red).

scaled by the standard deviation ($^{\circ}\text{C}$) of the iAMV index for a proper comparison of pattern amplitudes.] In contrast to the T&S method, the Residual method remains skillful for all end dates, with pattern correlations >0.97 (Figure 2a, red curve) and rmse values <0.3 (Figure 3a, red curve).

The decline of the pattern correlation and the rise of the rmse between the True and T&S-estimated iAMV patterns over the 21st century is associated with an increasing (inverse) resemblance between the T&S iAMV and forced trend patterns (Figure 2a, cyan curve). In particular, $r(\text{T\&S, forced trend})$ is negligible in the 2020s but reaches -0.85 in the 2060s, in tandem with the behavior of $r(\text{T\&S, true})$. This result supports the notion that as the forced trend pattern becomes more pronounced, it becomes progressively aliased onto the T&S estimate of iAMV. It should be noted that the true iAMV pattern has little projection on the forced trend regardless of the time period analyzed (Figure 2a, green curve).

As mentioned earlier, the nine model LEs used in our study have different ensemble sizes, ranging from 30 to 100 members (Table S1 in Supporting Information S1). Before turning to the results for the other models, we briefly investigate the sensitivity of the cumulative pattern correlations to ensemble size using the MPI

LE as a testbed. Repeating our analysis on three 30-member subsets (ensemble members 1–30, 31–60, and 61–90), we find qualitatively consistent results among the three, alleviating any major concerns regarding the effect of ensemble size discrepancy for our multi-model LE inter-comparison (Figure S14 in Supporting Information S1); similar conclusions hold for the other cumulative metrics (not shown).

Cumulative pattern correlation and rmse metrics for all nine model LEs are compared in Figures 2 and 3, respectively. In all models and for both metrics, the Residual method nearly always outperforms the T&S method (compare red and blue curves). The skill of the Residual method is evidenced by its high pattern correlation against the true iAMV ($r > 0.8$) for all end dates in all models, and rmse values generally ranging from 0.1 to 1.0 (with somewhat higher values in two of the models after about 2050: Figures 3h and 3i). In comparison, rmse values for the T&S method are generally 2–5 times higher than those for the Residual method, especially for the later end dates.

There is considerable model dependence to the character of the cumulative $r(\text{T\&S, true})$ curves, with some models exhibiting an evolution similar to MPI, albeit with different magnitudes and timing of the reduction relative to present-day, while others show more uniform values throughout the 21st century (Figure 2, blue curves). In addition, $r(\text{T\&S, forced trend})$ varies widely across models, with some showing values close to +1 and others close to -1 , depending on the time period (Figure 2, cyan curves). The disparate behavior in $r(\text{T\&S, forced trend})$ can be traced to the relative magnitudes of the forced trends in NA versus G. The models with a negative (positive) pattern correlation are those with a larger (smaller) amplitude of the forced trend in G compared to NA (not shown), due to how the T&S iAMV index is constructed (e.g., NA–G). Regardless, the spatial pattern of the forced trend is aliased onto the T&S estimate of iAMV, whether via NA or via –G. Finally, all models show generally modest pattern correlations (<0.3 in absolute value) between the true iAMV and the forced trend, except for CanESM5 which shows values around 0.6 regardless of time period (Figure 2, green curves; see also Figures S1–S9 in Supporting Information S1).

The results discussed above pertain to the full global (60°S – 60°N) domain. The reader is referred to Figures S10–S13 in Supporting Information S1 for the corresponding cumulative metrics calculated over just the NA region and over the global domain exclusive of the NA.

3.3. Assessing the Realism of Models' iAMV Patterns

How realistic are models' iAMV patterns? Figure 4 shows the observed (ERSSTv5) iAMV regression patterns estimated with the T&S and Residual methods over the period 1950–2020 (panels a and c, respectively). The two approaches yield very similar results, consistent with what was found for the models based on this time period. To evaluate the realism of the simulated iAMV patterns in each model LE, we compute the spatial correlation coefficient between the observed iAMV regression map estimated with the Residual method, and the model's true iAMV regression map obtained by averaging the true iAMV regression maps in each member to reduce the influence of sampling variability. We then compare these “ $r(\text{obs_resid, model_true})$ ” values to the distribution of “ $r(\text{model_resid, model_true})$ ” values obtained by computing the pattern correlation between the Residual estimate in each member with the ensemble-average of the model's true iAMV based on the period 1950–2020, analogous to our procedure for observations. The $r(\text{obs_resid, model_true})$ values based on ERSSTv5 and HadISST1 lie within the 5th–95th percentile range of the distribution of $r(\text{model_resid, model_true})$ values in each LE (Figure 4b). Repeating our procedure using rmse in place of pattern correlations, we find that the observed values generally lie well above the model distributions (in the upper tail for two of the models), and exceed the median value of each LE by a factor of 2–3 (Figure 4d). These results indicate that the models strongly underestimate the amplitude of the observed iAMV pattern based on the Residual method, consistent with previous studies (see Z19).

It is worth noting the large 5th-to-95th percentile ranges of these metrics across the model LEs (typically 0.2–0.7 for pattern correlations and a factor of 3 for rmse), underscoring that: (a) a single ensemble member from a given model LE is not sufficient to assess model fidelity of the global iAMV pattern, even with 70 years of data; and (b) the observed estimate of iAMV pattern may also be subject to large sampling fluctuations (e.g., the “true” iAMV pattern in the real world, obtained from a hypothetically infinite timeseries, might differ from the pattern estimated from the past 70 years of instrumental data). In this regard, we note that the observed iAMV regression map based on an independent period of record (1880–1950) exhibits

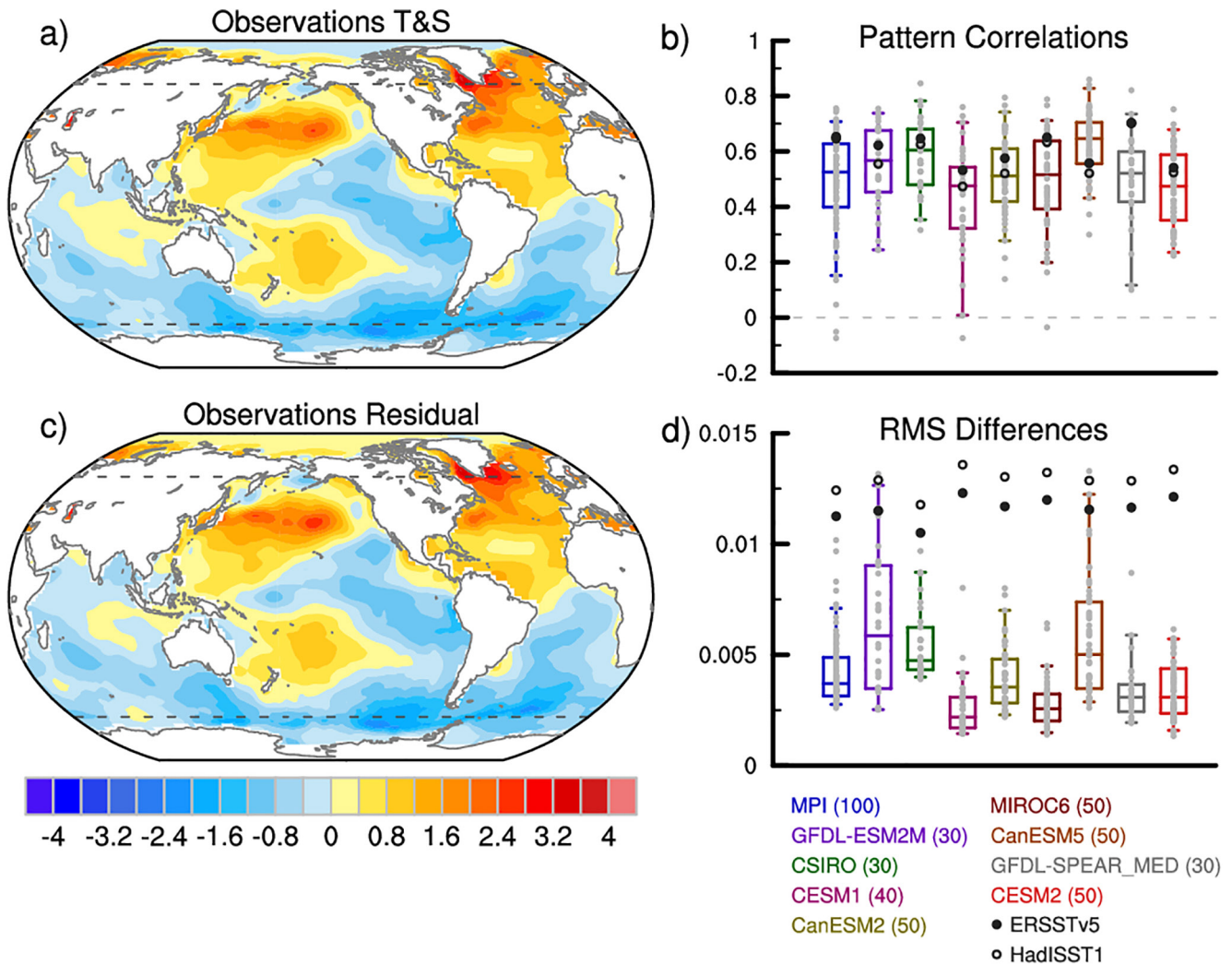


Figure 4. (Left) Observed (ERSSTv5) internal Atlantic Multidecadal Variability (iAMV) sea surface temperature regression map for 1950–2020 estimated with the (a) T&S and (c) Residual methods ($^{\circ}\text{C}$ per $^{\circ}\text{C}$ of the iAMV index). (Right) Distribution of (b) pattern correlations and (d) spatial rmse for each model between true and estimated (Residual method) iAMV in each member based on 1950–2020 (gray dots); box-and-whisker plots show the 5th–95th percentile range (whiskers), 25th–75th percentile range (box outlines) and the 50th percentile value (horizontal bar inside the box). Black circles show the pattern correlation and spatial rmse between observed (Residual method) iAMV (filled circles for ERSSTv5 and open circles for HadISST1) and the models' true iAMV.

some differences with the one based on 1950–2020, especially over data-sparse areas of the tropical Indo-Pacific and Southern Ocean (not shown).

4. Summary and Discussion

The canonical index of AMV is the low-pass filtered timeseries of SSTA averaged over the NA (e.g., Enfield et al., 2001; Z19). This index confounds externally forced climate change and internally generated climate variability. To isolate the contribution from internal variability, various methods have been employed, including linear detrending (Enfield et al., 2001), subtracting the global-mean SSTA (TS06) or subtracting the pattern of SSTA associated with global-mean temperature (the so-called “Residual” method: T09; Z19); more sophisticated approaches such as optimal fingerprinting (T09), optimal linear inverse modeling (Frankignoul et al., 2017) and low-frequency pattern recognition (Wills et al., 2020) have also been used. Here, we have evaluated the skill of the T&S and Residual methods in isolating the internal component of the global SSTA pattern of AMV, using a multi-model archive of LEs as a testbed in which the true internal

AMV pattern in each model is known *a priori* (via subtraction of the ensemble-mean). Our analysis examines the skill of each method under evolving anthropogenic climate change during the period 1940–2100.

We find that the T&S method aliases the structure of forced climate change onto the pattern and amplitude of internal AMV (iAMV) in all nine model LEs examined, especially by the mid-21st century. In contrast, the Residual method generally provides a skillful assessment of the spatial characteristics of iAMV in all models throughout the analysis period. The simulated patterns of iAMV during 1950–2020 are found to be realistic in all the LEs, but their amplitudes are biased low. However, there is considerable sampling uncertainty across the individual members of each LE, underscoring the challenge of evaluating low-frequency modes such as iAMV against a relatively short observational record.

Despite its excellent performance overall, the Residual method cannot accommodate changes in the forced pattern of SSTA (i.e., the SSTA pattern associated with the global-mean SSTA timeseries) that occur within the analysis period. Such changes may happen as a result of evolving sources of anthropogenic radiative forcing (for example, regional aerosol emissions), or as a result of feedbacks within the climate system that operate on different time scales, thereby modulating the regional pattern of response (e.g., Armour et al., 2016). This complexity underscores the need for more sophisticated approaches to determining the evolving pattern of the forced response (e.g., Frankignoul et al., 2017; Wills et al., 2020).

While it is beyond the scope of the present study to investigate the dynamical mechanisms governing the global SSTA pattern of iAMV in nature and in models, the definition of iAMV should ultimately be based on physical considerations. These physical considerations include stochastic atmospheric forcing of the ocean mixed layer and wind-driven ocean circulation, the role of AMOC in inducing subpolar SSTA, subsequent air-sea interactions that extend the SSTA into the tropical Atlantic, and atmospheric teleconnections that transmit the signal to other basins and trigger coupled interactions within the Pacific and beyond.

Data Availability Statement

All model simulations and observational data sets used in this study are publicly available. ERSSTv5 data is available from the NOAA-NCEI at <https://www.ncei.noaa.gov/products/extended-reconstructed-sst>. HadISST1 data is available from the UK Met Office Hadley Centre at <https://www.metoffice.gov.uk/hadobs/hadisst/index.html>. All CMIP5-class model data is available from the Multi-Model Large Ensemble Archive at <https://www.cesm.ucar.edu/projects/community-projects/MMLEA/>. All CMIP6 model data is available from the Earth System Grid Federation's Lawrence Livermore National Laboratory's data portal at <https://esgf-node.llnl.gov/search/cmip6/>. Analysis code is posted at cesm.ucar.edu/working_groups/CVC/cvdp-le/code.html.

References

- Armour, K. C., Marshall, J., Scott, J. R., Donohoe, A., & Newsom, E. R. (2016). Southern Ocean warming delayed by circumpolar upwelling and equatorward transport. *Nature Geoscience*, 9, 549–554. <https://doi.org/10.1038/ngeo2731>
- Bellomo, K., Murphy, L. N., Cane, M. A., Clement, A. C., & Polvani, L. M. (2018). Historical forcings as main drivers of the Atlantic multidecadal variability in the CESM large ensemble. *Climate Dynamics*, 50(9–10), 3687–3698. <https://doi.org/10.1007/s00382-017-3834-3>
- Booth, B. B., Dunstone, N. J., Halloran, P. R., Andrews, T., & Bellouin, N. (2012). Aerosols implicated as a prime driver of twentieth-century North Atlantic climate variability. *Nature*, 484(7393), 228–232. <https://doi.org/10.1038/nature10946>
- Buckley, M. W., Ponte, R. M., Forget, G., & Heimbach, P. (2014). Low-frequency SST and upper-ocean heat content variability in the North Atlantic. *Journal of Climate*, 27(27), 4996–5018. <https://doi.org/10.1175/JCLI-D-14-00523.1>
- Clement, A., Bellomo, K., Murphy, L. N., Cane, M. A., Mauritsen, T., Radel, G., & Stevens, B. (2015). The Atlantic multidecadal oscillation without a role for ocean circulation. *Science*, 350, 320–324. <https://doi.org/10.1126/science.aab3980>
- Delworth, T. L., Zeng, F., Zhang, L., Zhang, R., Vecchi, G. A., & Yang, X. (2017). The central role of ocean dynamics in connecting the North Atlantic Oscillation to the extratropical component of the Atlantic Multidecadal Oscillation. *Journal of Climate*, 30(10), 3789–3805. <https://doi.org/10.1175/JCLI-D-16-0358.1>
- Deser, C., Lehner, F., Rodgers, K. B., Ault, T., Delworth, T. L., DiNezio, P. N., et al. (2020). Insights from earth system model initial-condition large ensembles and future prospects. *Nature Climate Change*. <https://doi.org/10.1038/s41558-020-0731-2>
- Enfield, D. B., Mestas-Nuñez, A. M., & Trimble, P. J. (2001). The Atlantic multidecadal oscillation and its relation to rainfall and river flows in the continental US. *Geophysical Research Letters*, 28(10), 2077–2080. <https://doi.org/10.1029/2000GL012745>
- Frankignoul, C., Gastineau, G., & Kwon, Y. O. (2017). Estimation of the SST response to anthropogenic and external forcing and its impact on the Atlantic Multidecadal Oscillation and the Pacific Decadal Oscillation. *Journal of Climate*, 30(24), 9871–9895. <https://doi.org/10.1175/jcli-d-17-0009.1>

Acknowledgments

The authors thank the members of the NCAR's Climate Analysis Section for valuable discussions during the course of this work, and the anonymous Reviewers and the Editor for their constructive comments and suggestions. The authors also thank Dr. Stephen Yeager for assistance with python. This material is based upon work supported by the National Center for Atmospheric Research, which is a major facility sponsored by the National Science Foundation under cooperative agreement 1852977. The authors acknowledge high-performance computing support from Cheyenne (<https://doi.org/10.5065/D6RX99HX>) provided by the NCAR's Computational and Information Systems Laboratory, sponsored by the National Science Foundation.

- Huang, B., Thorne, P. W., Banzon, V. F., Boyer, T., Chepurin, G., Lawrimore, J. H., et al. (2017). Extended reconstructed sea surface temperature, version 5 (ERSSTv5): Upgrades, validations, and intercomparisons. *Journal of Climate*, *30*(20), 8179–8205. <https://doi.org/10.1175/jcli-d-16-0836.1>
- Kim, W. M., Yeager, S., & Danabasoglu, G. (2020). Atlantic Multidecadal Variability and associated climate impacts initiated by ocean thermohaline dynamics. *Journal of Climate*, *33*(4), 13171334. <https://doi.org/10.1175/jcli-d-19-0530.1>
- Kim, W. M., Yeager, S. G., & Danabasoglu, G. (2018). Key role of internal ocean dynamics in Atlantic Multidecadal Variability during the last half century. *Geophysical Research Letters*, *45*, 13449–13457. <https://doi.org/10.1029/2018GL080474>
- Mann, M. E., Steinman, B. A., & Miller, S. K. (2020). Absence of internal multidecadal and interdecadal oscillations in climate model simulations. *Nature Communications*, *11*, 49. <https://doi.org/10.1038/s41467-019-13823-w>
- Murphy, L. N., Bellomo, K., Cane, M., & Clement, A. (2017). The role of historical forcings in simulating the observed Atlantic multidecadal oscillation. *Geophysical Research Letters*, *44*, 2472–2480. <https://doi.org/10.1002/2016GL071337>
- Newman, M., Alexander, M. A., Ault, T. R., Cobb, K. M., Deser, C., Di Lorenzo, E., et al. (2016). The Pacific decadal oscillation, revisited. *Journal of Climate*, *29*, 4399–4427. <https://doi.org/10.1175/JCLI-D-15-0508.1>
- Qin, M., Dai, A., & Hua, W. (2020). Quantifying contributions of internal variability and external forcing to Atlantic Multidecadal Variability since 1870. *Geophysical Research Letters*, *47*, e2020GL089504. <https://doi.org/10.1029/2020GL089504>
- Rayner, N. A., Parker, D. E., Horton, E. B., Folland, C. K., Alexander, L. V., Rowell, D. P., et al. (2003). Global analyses of sea surface temperature, sea ice, and night marine air temperature since the late nineteenth century. *Journal of Geophysical Research*, *108*(D14), 4407. <https://doi.org/10.1029/2002JD002670>
- Simpson, I. R., Deser, C., McKinnon, K. A., & Barnes, E. A. (2018). Modelled and observed multidecadal variability in the North Atlantic jet stream and its connection to sea surface temperatures. *Journal of Climate*, 8313–8338. <https://doi.org/10.1175/JCLI-D-18-0168.1>
- Ting, M., Kushnir, Y., Seager, R., & Li, C. (2009). Forced and internal twentieth-century SST trends in the North Atlantic. *Journal of Climate*, *22*(6), 1469–1481. <https://doi.org/10.1175/2008JCLI2561.1>
- Trenberth, K. E., & Shea, D. J. (2006). Atlantic hurricanes and natural variability in 2005. *Geophysical Research Letters*, *33*, L12704. <https://doi.org/10.1029/2006GL026894>
- Wills, R. C., Armour, K. C., Battisti, D. S., & Hartmann, D. L. (2019). Ocean–atmosphere dynamical coupling fundamental to the Atlantic Multidecadal Oscillation. *Journal of Climate*, *32*(1), 251–272. <https://doi.org/10.1175/JCLI-D-18-0269.1>
- Wills, R. C. J., Battisti, D. S., Armour, K. C., Schneider, T., & Deser, C. (2020). Pattern recognition methods to separate forced responses from internal variability in climate model ensembles and observations. *Journal of Climate*, *33*, 8693–8719. <https://doi.org/10.1175/jcli-d-19-0855.1>
- Yan, X., Zhang, R., & Knutson, T. R. (2019). A multivariate AMV index and associated discrepancies between observed and CMIP5 externally forced AMV. *Geophysical Research Letters*, *46*, 4421–4431. <https://doi.org/10.1029/2019GL082787>
- Zhang, R., Sutton, R., Danabasoglu, G., Kwon, Y.-O., Marsh, R., Yeager, S. G., et al. (2019). A 456 review of the role of the Atlantic Meridional Overturning Circulation in Atlantic Multidecadal Variability and associated climate impacts. *Reviews of Geophysics*, *57*, 316–375. <https://doi.org/10.1029/2019RG000644>

References From the Supporting Information

- Delworth, T. L., Cooke, W. F., Adcroft, A., Bushuk, M., Chen, J.-H., Dunne, K. A., et al. (2020). SPEAR: The next generation GFDL modeling system for seasonal to multidecadal prediction and projection. *Journal of Advances in Modeling Earth Systems*, *12*, e2019MS001895. <https://doi.org/10.1029/2019MS001895>
- Jeffrey, S., Rotstayn, L., Collier, M., Dravitzki, S., Hamalainen, C., Moeseneder, C., et al. (2013). Australia's CMIP5 submission using the CSIRO-Mk3.6 model. *Australian Meteorological and Oceanographic Journal*, *63*, 1–13. <https://doi.org/10.22499/2.6301.001>
- Kay, J. E., Deser, C., Phillips, A., Mai, A., Hannay, C., Strand, G., et al. (2015). The Community Earth System Model (CESM) Large Ensemble Project: A community resource for studying climate change in the presence of internal climate variability. *Bulletin of the American Meteorological Society*, *96*, 1333–1349. <https://doi.org/10.1175/BAMS-D-13-00255.1>
- Kirchmeier-Young, M. C., Zwiers, F. W., & Gillett, N. P. (2017). Attribution of extreme events in Arctic Sea ice extent. *Journal of Climate*, *30*, 553–571. <https://doi.org/10.1175/jcli-d-16-0412.1>
- Maher, N., Milinski, S., Suarez-Gutierrez, L., Botzet, M., Dobrynin, M., Kornblueh, L., et al. (2019). The Max Planck Institute Grand Ensemble: Enabling the exploration of climate system variability. *Journal of Advances in Modeling Earth Systems*, *11*, 2050–2069. <https://doi.org/10.1029/2019MS001639>
- Rodgers, K. B., Lin, J., & Frölicher, T. L. (2015). Emergence of multiple ocean ecosystem drivers in a large ensemble suite with an Earth system model. *Biogeosciences*, *12*, 3301–3320. <https://doi.org/10.5194/bg-12-3301-2015>
- Swart, N. C., Cole, J. N. S., Kharin, V. V., Lazare, M., Scinocca, J. F., Gillett, N. P., et al. (2019). The Canadian Earth System Model version 5 (CanESM5.0.3). *Geoscientific Model Development*, *12*, 4823–4873. <https://doi.org/10.5194/gmd-12-4823-2019>
- Tatebe, H., Ogura, T., Nitta, T., Komuro, Y., Ogochi, K., Takemura, T., et al. (2019). Description and basic evaluation of simulated mean state, internal variability, and climate sensitivity in MIROC6. *Geoscientific Model Development*, *12*(7), 2727–2765. <https://doi.org/10.5194/gmd-12-2727-2019>